

Toward noninvasive measurement of blood hematocrit using spectral domain low coherence interferometry and retinal tracking

**Nicușor V. Iftimia
Daniel X. Hammer
Chad E. Bigelow
David I. Rosen
Teoman Ustun
Anthony A. Ferrante
Danhu Vu
R. Daniel Ferguson**

Nicușor V. Iftimia, Daniel X. Hammer, Chad E. Bigelow, David I. Rosen, Teoman Ustun, Anthony A. Ferrante, Danhu Vu, R. Daniel Ferguson, "Toward noninvasive measurement of blood hematocrit using spectral domain low coherence interferometry and retinal tracking ,"*Optics Express* **14**(8), 3377-3388 (April2006).

Copyright © 2006, [Optical Society of America](#). All rights reserved.

Reprinted by permission of the Optical Society of America. For permission to copy or republish, contact the Optical Society of America, 2010 Massachusetts Ave. NW, Washington, DC 20036-1023.

Toward noninvasive measurement of blood hematocrit using spectral domain low coherence interferometry and retinal tracking

Nicusor V. Iftimia, Daniel X. Hammer, Chad E. Bigelow, David I. Rosen, Teoman Ustun,
Anthony A. Ferrante, Danthu Vu, and R. Daniel Ferguson

Physical Sciences. Inc, 20 New England Business Ctr. Drive, Andover, MA 01810
iftimia@psicorp.com, ferguson@psicorp.com

Abstract: We demonstrate *in vivo* measurements in human retinal vessels of an experimental parameter, the slope of the low coherence interferometry (LCI) depth reflectivity profile, which strongly correlates with the real value of blood hematocrit. A novel instrument that combines two technologies, spectral domain low coherence interferometry (SDLCI) and retinal tracking, has been developed and used for these measurements. Retinal tracking allows a light beam to be stabilized on retinal vessels, while SDLCI is used for obtaining depth-reflectivity profiles within the investigated vessel. SDLCI backscatter extinction rates are obtained from the initial slope of the A-scan profile within the vessel lumen. The differences in the slopes of the depth reflectivity profiles for different subjects are interpreted as the difference in the scattering coefficient, which is correlated with the number density of red blood cells (RBC) in blood. With proper calibration, it is possible to determine hematocrit in retinal vessels. *Ex vivo* measurements at various RBC concentrations were performed to calibrate the instrument. Preliminary measurements on several healthy volunteers show estimated hematocrit values within the normal clinical range.

2005 Optical Society of America

OCIS codes: (170.3880) Medical and biological imaging; (120.3890) Medical optics instrumentation.

References and links

1. C. Johner, P. Chamney, D. Schneditz, and M. Krämer, "Evaluation of an ultrasonic blood volume monitor", *Nephrol. Dial. Transplant.* **13**, 2098–2103 (1998).
2. W. Secomsky, A. Nowicki, F. Guidi, P. Tortoli, and P.A. Lewin, "Non-invasive measurement of blood hematocrit in artery", *Bulletin of the Polish Academy of Sciences*, **53** (3), 245-50 (2005).
3. J.M. Schmitt, Z. Guan-Xiong, and J. Miller, "Measurement of blood hematocrit by dual-wavelength near-IR photoplethysmography", *Proc. SPIE* **1441**, 150-161 (1992).
4. A. F. Fercher, W. Drexler, C. K. Hitzenberger and T. Lasser, "Optical coherence tomography- principles and application," *Rep. Prog. Phys.* **66**, 239-303 (2003).
5. R. Leitgeb, C. K. Hitzenberger, and A. F. Fercher, "Performance of Fourier domain vs. time domain optical coherence tomography," *Opt. Express* **11**, 889-894 (2003), <http://www.opticsexpress.org/abstract.cfm?URI=OPEX-11-8-889>.
6. S. H. Yun, G. J. Tearney, J. F. de Boer, N. Iftimia, and B. E. Bouma, "High-speed optical frequency-domain imaging," *Opt. Express* **11**, 2953-2963 (2003), <http://www.opticsexpress.org/abstract.cfm?URI=OPEX-11-22-2953>.
7. J.F. de Boer, B. Cense, B.H. Park, et al., "Improved signal-to-noise ratio in spectral-domain compared with timedomain optical coherence tomography," *Opt. Lett.* **28**, 2067-2069 (2003).
8. N.A. Nassif, B. Cense, B.H. Park, et al., "In vivo high-resolution video-rate spectral-domain optical coherence tomography of the human retina and optic nerve," *Opt. Express* **12**, 367-376 (2004), <http://www.opticsexpress.org/abstract.cfm?URI=OPEX-12-3-367>.
9. A. Gh. Podoleanu, M. Seeger, G. M. Dobre, D. J. Webb, D. A. Jackson and F. Fitzke, "Transversal and longitudinal images from the retina of the living eye using low coherence reflectometry," *J. Biomed. Opt.* **3**, 12- (1998).
10. H. Liang, M. G. Cid, R. G. Cucu, G. M. Dobre, A. G. Podoleanu, J. Pedro, and D. Saunders, "En-face optical coherence tomography – a novel application of non-invasive imaging to art conservation," *Opt. Express* **13**, 6133-6144 (2005), <http://www.opticsexpress.org/abstract.cfm?URI=OPEX-13-16-6133>.

11. B.R. White, M.C. Pierce, N. Nassif, et al., "In vivo dynamic human retinal blood flow imaging using ultra-highspeed spectral domain optical Doppler tomography," Opt. Express **11**, 3490-3497 (2004), <http://www.opticsexpress.org/abstract.cfm?URI=OPEX-11-25-3490>.
12. J. Zhang and Z. Chen, "In vivo blood flow imaging by a swept laser source based Fourier domain optical Doppler tomography," Opt. Express **13**, 7449-7457 (2005), <http://www.opticsexpress.org/abstract.cfm?URI=OPEX-13-19-7449>.
13. C. Xu, D. L. Marks, M. N. Do, and S. A. Boppart, "Separation of absorption and scattering profiles in spectroscopic optical coherence tomography using a least-squares algorithm," Opt. Express **12**, 4790-4803 (2004), <http://www.opticsexpress.org/abstract.cfm?URI=OPEX-12-20-4790>.
14. B. Hermann, K. Bizheva, A. Unterhuber, B. Povazay, H. Sattmann, L. Schmetterer, A. F. Fercher and W. Drexler, "Precision of extracting absorption profiles from weakly scattering media with spectroscopic time-domain optical coherence tomography," Opt. Express **12**, 1677-1688 (2004).
15. D. X. Hammer, R. D. Ferguson, N. V. Iftimia, T. Ustun, G. Wollstein, H. Ishikawa, M. L. Gabriele, W. D. Dilworth, L. Kagemann, and J. S. Schuman, "Advanced scanning methods with tracking optical coherence tomography," Opt. Express **13**, 7937-7947 (2005), <http://www.opticsexpress.org/abstract.cfm?URI=OPEX-13-20-7937>.
16. D. P. Wornson, G. W. Hughes, and R. H. Webb, "Fundus tracking with the scanning laser ophthalmoscope," Appl. Opt. **26**, 1500-1504 (1987).
17. T. N. Cornsweet and H. D. Crane, "Servo-controlled infrared optometer," J. Opt. Soc. Am. **60**, 548-554 (1970).
18. M Yu Kirillin, A.V. Priezzhev, V V Tuchin, R K Wang, and R Myllylä, "Effect of red blood cell aggregation and sedimentation on optical coherence tomography signals from blood samples", *J. Phys. D: Appl. Phys.* **38** 2582-2589 (2005).
19. D. X. Hammer, R. D. Ferguson, J. C. Magill, M. A. White, A. E. Elsner, and R. H. Webb, "Image stabilization for scanning laser ophthalmoscopy," Opt. Express **10**, 1542-1549 (2002), <http://www.opticsexpress.org/abstract.cfm?URI=OPEX-10-26-1542>.
20. G. Hausler and M. W. Lindner, "Coherence radar and spectral radar - new tools for dermatological diagnosis," J. Biomed. Opt. **3**, 21-31 (1998).
21. M. Wojtkowski, V. J. Srinivasan, T. H. Ko, J. G. Fujimoto, A. Kowalczyk, and J. S. Duker, "Ultrahigh-resolution, high-speed, Fourier domain optical coherence tomography and methods for dispersion compensation," Opt. Express **12**, 2404-2422 (2004), <http://www.opticsexpress.org/abstract.cfm?URI=OPEX-12-11-2404>.
22. L. Thrahe, M.H. Frosz, T.M. Jørgensen, A. Tycho, H.T. Yura, P.E. Andersen, " Extraction of optical scattering parameters and attenuation compensation in optical coherence tomography images of multilayered tissue structures", Opt. Lett. **29**(14), 1641-43 (2004).
23. D. J. Faber, E.G. Mick, M.C.G. Aalders, T.G. van Leeuwen, "Light absorption of (oxy)-hemoglobin assessed by spectroscopic optical coherence tomography", Opt. Lett **28**(16), 1436-38 (2003).
24. D. J. Faber, E.G. Mick, M.C.G. Aalders, T.G. van Leeuwen, "Toward assessment of blood oxygen saturation by spectroscopic optical coherence tomography", Opt. Lett. **30**(9), 1015-17 (2005).
25. J.M. Steinke and A.P. Shepherd, "Diffusion model of the optical absorbance of whole blood", J. Opt. Soc. Am. A **5**, 813-822 (1988).
26. A. Roggan, M. Friebel, K. Dörschel, A. Hahn, and G. Müller, "Optical Properties of Circulating Human Blood in the Wavelength Range 400–2500 nm", Journal of Biomedical Optics **4**(1), 36-46 (1999).

1. Introduction

Blood hematocrit is defined as the volume percentage of the blood that consists of red blood cells (RBC's). Non-invasive monitoring of hematocrit would be quite valuable for many clinical applications. Rapid determination of hematocrit, on a periodic or continuous monitoring is essential for patients with blood disorders, in emergency situations, post operatively, or with therapies that compromise blood-forming functions and organs.

Several noninvasive methods have been proposed for hematocrit measurements. Ultrasound-based continuous hematocrit measurement has been proposed by Johner et al. [1]. They determined the value of hematocrit by monitoring changes in ultrasound wave velocity propagation in plasma as a function of RBC's concentration. Although they reported good correlation between their measurements and the real value of the hematocrit, they noted that the uncertainty of the method depended markedly on even minute temperature variations. A Doppler ultrasound method has been tested as well by Secomski et al. [2]. Their results demonstrated that hematocrit could be non-invasively determined in the brachial artery to within an error of 5%. However, it was observed that the lateral movement of the vessel induces additional errors. To keep the error within 5% very sophisticated multiple gated Doppler circuitry was necessary. Near infrared (NIR) optical imaging of the blood vessels

through skin has been tested by Schmitt et al. [3] for noninvasive hematocrit measurement. Unfortunately, lack of direct access to blood vessels alters the result of the measurements due to the variation of the skin's optical properties from one person to another.

In this paper we show noninvasive estimation of blood hematocrit by using low coherence interferometry (LCI) and directly accessing small vessels of the retina. The slope of the LCI depth reflectivity profile is used to determine hematocrit information.

LCI has become a powerful technique that is largely used in optical coherence tomography (OCT) to obtain cross sectional images of biological tissues. Standard OCT images are based on the intensity of backscattered or backreflected optical radiation. In the standard time-domain (TD) implementation of LCI, a mirror is rapidly scanned in the reference arm of the interferometer in order to obtain a depth reflectivity profile within a sample. An alternative method of retrieving depth information examines the cross-spectral density to reconstruct the interferogram by detecting the interference signal as a function of wavelength [4,5]. This method, known as spectral-domain (SD) LCI, does not require modulation of the reference arm length and therefore has potential for faster acquisition rates. Although this method was demonstrated years ago, only recently has it been explicitly shown that SD implementation of OCT (and LCI) has vastly superior detection sensitivity compared to the time domain method. Recent work has experimentally demonstrated a 148-fold (21.7 dB) sensitivity improvement with SDOCT [6].

SDLCI is used in ophthalmology to obtain cross-sectional or en face images of the retina [7-9], to measure Doppler flow in the retinal vessels [10,11], or for spectroscopic measurements [12,13]. However, due to the strong forward scattering of blood, SDLCI measurements require relatively long exposure durations to collect enough photons to achieve adequate signal-to-noise levels within the confines of laser safety requirements. Unfortunately, eye movement makes such measurements difficult. The light beam interrogating the eye must be stabilized on a fixed location on a specific retinal vessel to collect reproducible depth-reflectivity profiles in the blood. This is possible only by employing an eye motion stabilization technique. Eye motion stabilization can generally be accomplished invasively with suction cups or retrobulbar injections, inaccurately with fixation, more precisely at slower speeds with a passive image processing approach, or at high speeds with active tracking [14,15]. Fixation requires patient cooperation and is difficult in patients with poor vision. Other active tracking techniques, such as double-Purkinje trackers [16,17], are specifically designed for the anterior segment and are less reliable for measurement of retinal position.

We demonstrate that the combination of two technologies, direct retinal tracking with tracking scanning laser ophthalmoscopy (TSLO), and SDLCI, is suitable for non-invasive measurement of blood hematocrit level (H). Preliminary measurements on several volunteers show that noninvasive blood hematocrit estimates correlate well with conventional clinical methods.

2. Methods and materials

2.1. Theoretical approach

To illustrate the basic methodology, a relatively simple theoretical model was used to extract the hematocrit level from the depth (axial) reflectivity profile by simply measuring its slope and applying a scaling factor. The amplitude S of the LCI fringes is proportional to the square root of the light intensities I_s and I_r returning from the sample and the reference arm of the interferometer, respectively:

$$S_{LCI}(z) = k[I_r I_s(\lambda, z)]^{1/2}, \quad (1)$$

k denotes a constant factor that is given by the LCI system specifications (e.g. detector responsitivity). $I_s(\lambda, z)$ depends on the reflectivity of the sample at a depth z within the sample,

the signal intensity caused by coherent superposition of the electromagnetic fields from different scatters within the coherence volume, and the position of the focal spot within the sample.

The intensity of the light from the sample arm that propagates through the sample can be described by Beer's law:

$$I_s(\lambda, z) = I_{s0}(\lambda) \exp\{-[\mu_a(\lambda, z) + \mu_s(\lambda, z)]z\}, \quad (2)$$

where I_{s0} denotes the incident intensity, λ the wavelength, μ_a the absorption coefficient, and μ_s the total scattering coefficient. However, for the SDLCI case, mostly singly scattered photons are detected. Some multiple scattered photons fall within the coherence gate with a measurable contribution to the slope of the SDLCI depth reflectivity profile. As a result, the experimental slope of the LCI reflectivity profile is reduced: neither the true scattering coefficient μ_s , nor the reduced value μ'_s is actually appropriate for our calculation. With the provision that μ_s is actually a bandwidth-dependent parameter, μ_{s-LCI} , if we take the logarithm of Eq. (1) and use Eq. (2) we obtain:

$$\ln[S_{LCI}(z)] = \ln\{k[I_r(\lambda)I_{s0}(\lambda)]^{1/2}\} - \{[\mu_a(\lambda, z) + \mu_{s-LCI}(\lambda, z)]z\} \quad (3)$$

where we have taken into account the double pass configuration of the LCI signal.

With the assumption of a constant incident and reference intensity, eq. (3) is a linear function in z and the initial slope s in the lumen is given by:

$$s = -[\mu_a(\lambda, z) + \mu_{s-LCI}(\lambda, z)] \quad (4)$$

By choosing a light source with the central wavelength within the 700 nm to 900 nm spectral interval, where the absorption coefficient of light in blood is small compared to the total scattering coefficient, the influence of μ_a in eq. (4) is minimized and can be regarded as an approximately constant factor. Measurements performed by other research groups [18,19] show that at around 800 nm μ_a is almost two orders of magnitude lower than μ_s ($\mu_a \approx 0.82 \text{ mm}^{-1}$, $\mu_s \approx 57 \text{ mm}^{-1}$). Slope changes in eq. (4) are therefore a direct measure of the scattering coefficient, μ_{s-LCI} , which depends upon the volume fraction of RBC's (i.e. hematocrit).

Based on the above arguments, the hematocrit level can be estimated directly by measuring the slope of the LCI depth reflectivity profile and applying a scaling factor determined from blood samples with a known hematocrit value. However, second order corrections will be required for significantly microcytic or macrocytic cells.

2. 2. Instrumentation

In principle, *in vivo* hematocrit measurements can be performed with an SD-LCI instrument and a camera for ocular fundus imaging. However, in order to stabilize the beam on the retinal vessel, a retinal motion tracker is necessary. A tracking scanning laser ophthalmoscope (TSLO) and an SDLCI/OCT system were integrated into a single platform. The schematic of the TSLO/SDLCI instrument is shown in Fig. 1.

TSLO is used to provide an image of the retina and stabilize the SDLCI/OCT beam on retinal vessels. The TSLO system consists of a custom-designed confocal line scanning laser ophthalmoscope (LSLO) and a retinal tracker. A complete description of these systems can be found elsewhere [15,19].

The LSLO portion of the system consists of an illumination source (940 nm laser diode-RLT9510MG, Roithner LaserTechnik, Austria), a custom-made confocal reflectometer, a linear array CMOS detector (PDI-1200, Fairchild Imaging), a scanner (Model 6200H, Cambridge Technology, Inc.), and imaging lenses (scan lens and ophthalmoscopic lens). For

LSLO imaging, less than 0.5 mW from the laser diode is incident on the eye. The line scanner simultaneously scans a line across the ocular fundus and de-scans the backscattered return onto a custom linear CMOS array camera. Since the LSLO uses confocal line illumination rather than a flying spot design, it is confocal in only one dimension.

The retinal tracking portion of the instrument consists of a confocal tracking reflectometer, dither scanners (16 kHz resonant scanners, Electro-Optical Products Corporation), and two tracking galvanometers (Model 6220H, Cambridge Technology, Inc.). The system works by steering the entire image raster produced by the imaging galvanometer with the motion of the eye using tracking mirrors. A tracking beam, locked onto a retinal feature, senses the motion of the eye. The confocal reflectometer is used to collect only light reflected from the plane of the fundus. The error signals generated by the system are therefore not affected by reflections from the cornea and lens. The source for the tracker beam is a 1064 nm light-emitting diode (RLT1060-10MG, Roithner LaserTechnik, Austria) coupled to a single mode fiber. The power of the diode is adjusted such that the tracker beam power that reaches the cornea is slightly less than 100 μ W. A PIN InGaAs photo-diode (PerkinElmer, model C30619G), connected to a custom-made low noise/high gain transimpedance amplifier, is used to detect the weak reflectance signal. The tracking beam is dithered in a circle with dither scanners driven at their resonant frequency of about 16 kHz and with 90° phase separation between x and y scanners. When the tracking beam passes over a retinal feature with brightness different from the background, the retro-reflected signal contains a 16-kHz signal, the phase and amplitude of which are determined by the direction and displacement of the tracking beam with respect to the feature. Phase-sensitive detection with a lock-in amplifier is employed to create error signals, which are then fed into a DSP feedback control loop (tracking module). The control loop drives the tracking galvanometers so that the imaging raster and SDLCI/OCT beams remain locked to the retina.

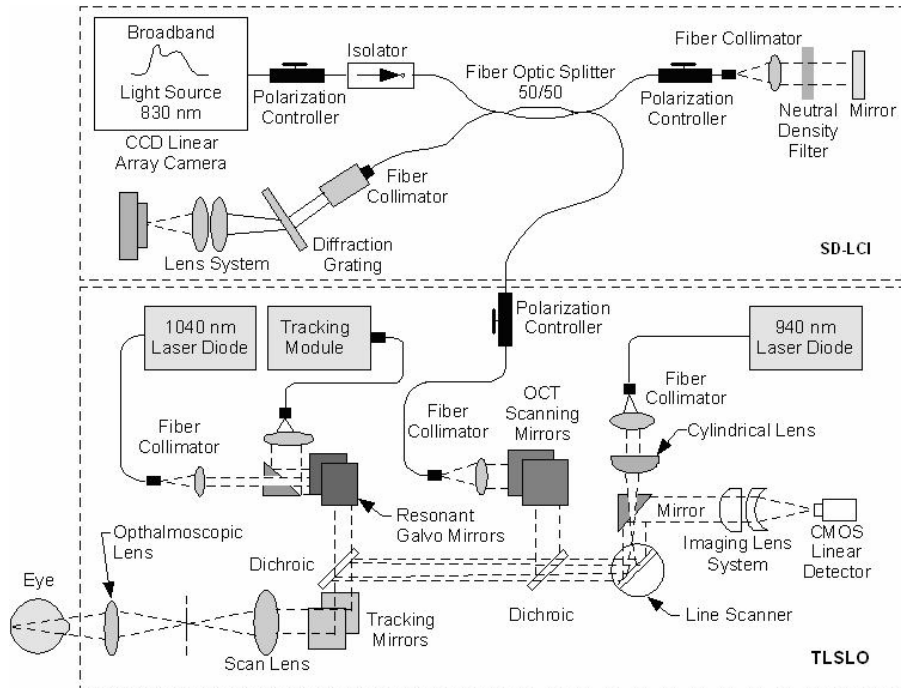


Fig. 1. General optical layout of the TSLO/SDLCI instrument.

The SD-LCI/OCT system consists of a broadband light source, a fiber-optic interferometer, and a spectral detection and data processing unit. A broadband superluminescent diode (SLD-37MP, Superlum-Russia) with 830 nm central wavelength and 50 nm bandwidth is used as a light source. According to eq. (5), the theoretical axial resolution l_z obtained with this light source is $\sim 6 \mu\text{m}$ in air and $\sim 4.5 \mu\text{m}$ in biological tissue: [20]

$$l_z = 0.44 \frac{\lambda_0^2}{n\Delta\lambda}, \quad (5)$$

where λ_0 is the center wavelength, $\Delta\lambda$ is the spectral width of the light source, and n is the refractive index of the sample.

The fiber optic interferometer consists of a 50/50 fiber optic beam-splitter that has four arms: the illumination arm, the sample arm, the reference arm, and the detection arm. Light from the light source is split in two within the sample and reference arms. A fraction of the light transmitted to the sample arm is backscattered from the sample, passes back into the interferometer and mixes with the reference beam. This light passes back to the input arms, being equally split between the detector arm and the illumination arm. An isolator is placed in the illumination arm to prevent this light from going back to the light source. An optical delay line (ODL), consisting of a mirror placed on a translation stage and a neutral density filter (NDF) is placed in the reference arm to match the length of the sample arm. The polarization of the reference beam is adjusted with a paddle polarization controller to match the polarization of the light from the sample arm. This adjustment ensures that polarization changes caused by bending and rotation of the optical fiber in both the sample and reference arms do not wash out the interference fringes.

The core of the SDLCI/OCT system is the spectral detection unit. The optical spectrum is dispersed by a holographic diffraction grating (Wasatch Photonics, 1200 lines per mm) and imaged by a custom designed lens system onto a Silicon CCD array line scan camera (L104k, Basler Vision, Inc.). The CCD has 1024 detector pixels with a 10 μm pitch and can operate at a maximum line readout rate of 58.5 kHz. Spectrometer resolution, $\delta\lambda$, of about 0.2 nm was obtained. The output of the camera is digitized by a camera link board (NI PCI-1429). The sampled data are transferred continuously to computer memory. The usual λ to ω (or k) interpolation was performed for our spectrometer. A discrete Fourier transform (DFT) is performed on each set of 1024 data points acquired by the CCD to produce an axial depth profile of the sample (A-line). Using this system a penetration depth of about 750 microns was possible in retinal tissue at a SNR of about 100 dB.

The LCI beam is sent to the eye by means of a scanning mirror pair that allows for beam positioning on the desired retinal vessel. These mirrors can also be used to scan the beam across the retina and generate OCT images.

The TSLO/SD-LCI system is controlled by a P4/3 GHz computer using LabView software. An interactive graphic user interface (GUI), shown in Figure 2, is used for setting system parameters, data acquisition, processing, and storage.

In order to achieve the optimal resolution consistent with the light source bandwidth, it was necessary to carefully match dispersion between the two arms of the interferometer. The standard technique balances the dispersion of the sample by arranging a dispersive material in the reference arm. However, this method requires adjustment from one sample to another. Our numeric dispersion algorithm enables automatic dispersion correction of depth reflectivity profiles at different positions with the eye. A Hilbert transform is used to calculate the complex representation of the light source spectrum and determine the phase function. The phase of the signal is modified by a polynomial equation in an iterative loop. A similar

approach was described by M. Wojtkowski et al. [21] for automatic dispersion compensation in high resolution OCT imaging. They used the sharpness of the image as criterion for optimum dispersion compensation. We use the variance of each A-line summed over the local OCT image frame as the objective function to be maximized. A schematic of this algorithm is shown in Figure 3. The phase, $\phi(\omega)$, of the signal is iteratively corrected until the variance of the depth reflectivity profiles are maximized. Once the locally correct phase function has been calculated, the spectra are reconstructed and Fast Fourier transformed to derive the corrected depth reflectivity LCI profiles in real time. LCI “M-scans” (a single A-line repeatedly acquired in time without transverse scanning) are automatically segmented and average slopes in the lumen are obtained.

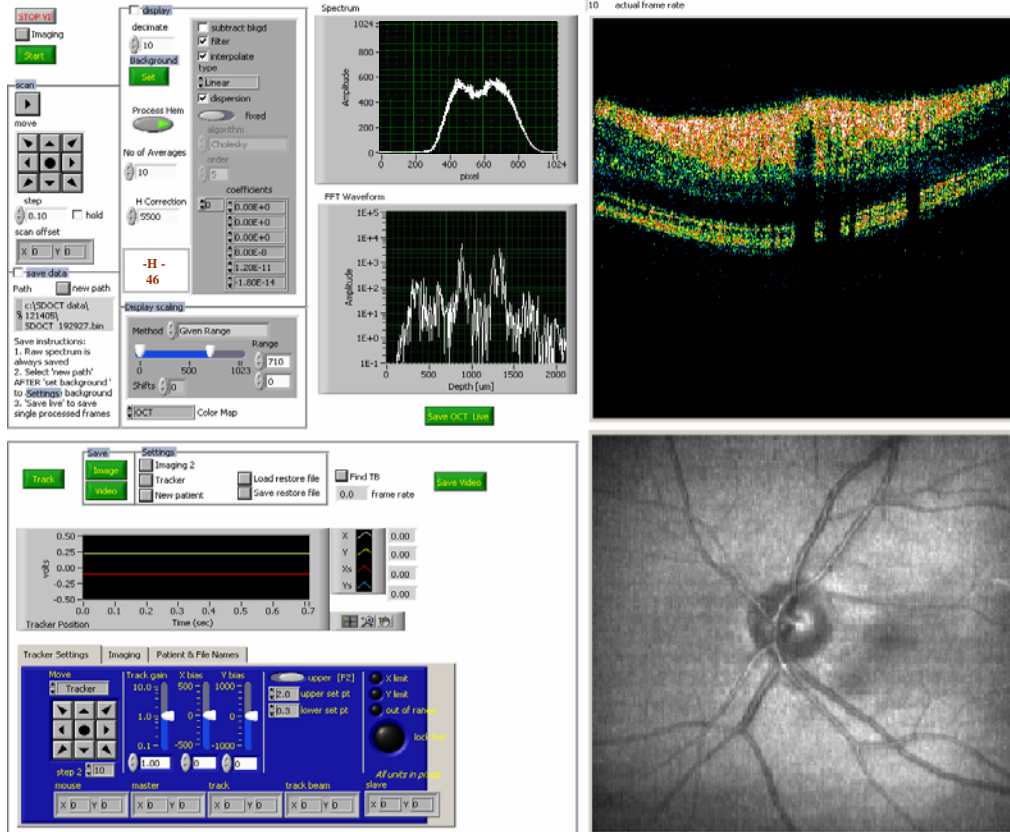


Fig. 2. TLSLO/SDLCI GUI interface

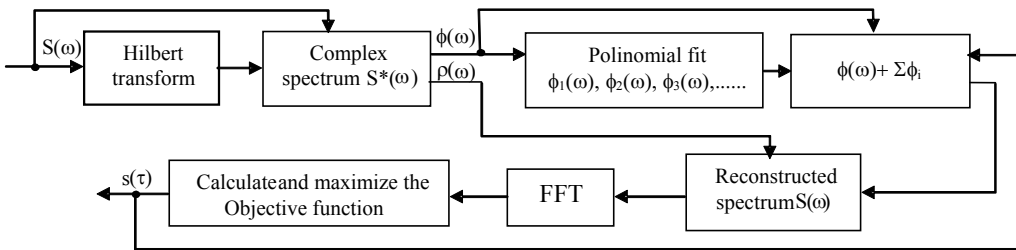


Fig. 3. Schematic of the automated dispersion compensation algorithm.

A model eye with a partially reflecting mirror at the back end was filled with water and used to test the effectiveness of our dispersion compensation algorithm. The axial point spread function (PSF) with the dispersion correction turned “off” and “on” is shown in Figure 4. The full-width at half maximum (FWHM) of the axial PSF was approximately 6.0 μm with dispersion correction and slightly over 17 μm without dispersion correction. The small discrepancy between the experimental and the theoretical FWHM values may be attributed to aberrations of the spectrometer or to insufficiently high order of the polynomial fit.

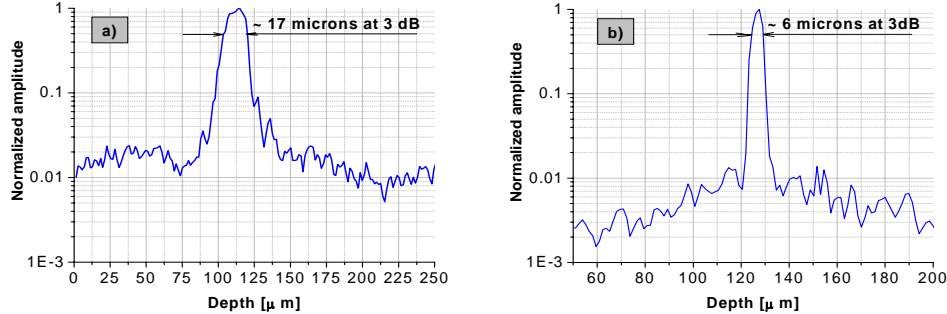


Fig. 4. The axial PSF (normalized power spectrum of the interference fringes), a) without dispersion compensation and b) with dispersion compensation

3. Results and discussion

Optical properties of blood are difficult to be determined with LCI (OCT) since several factors, like the anisotropy factor g , the O_2 -saturation dependent scattering, the contribution of multiply scattered photons [22], and wavelength dependence of the absorption coefficient [23,24] can substantially affect the results of the measurements.

In general, the effects of anisotropy and multiple scattering are difficult to compensate [22]. However, these effects would be expected to be constant factors in normo-cytic subjects, and thus able to be calibrated. It is also well known that the scattering coefficient is not linearly dependent with H , as described by J.M. Schmitt [3], and modeled by Steinke [25]. However, it has been shown that for H values up to about 55%, the strength of the backscattered signal is proportional with the RBC number density and the mean corpuscular volume (MCV) [3,26].

The O_2 -saturation dependence of scattering and the wavelength dependence of the absorption can be minimized by choosing the SDLCI band near the isobestic point (~805nm). At normal physiologic oxygen tension in arterial blood, this effect has, in general, a small systematic effect with even smaller inter- and intra-subjects variation.

SDLCI system parameters, like focusing depth, spectrometer linearity, etc. can also affect the results of the measurements. However, a careful calibration of the system can eliminate the effects of these factors.

3. 1 *In vitro* study

In vitro measurements on sheep blood samples (Hemostat Laboratories) were performed with our instrument. The goal of the *ex vivo* study was to evaluate the effects of both system parameters and blood on the results of the measurements, to calibrate the system, and evaluate its capability to discriminate between different hematocrit levels.

Various hematocrit levels were obtained by mixing whole blood with blood serum obtained through centrifugation. The hematocrit of each blood sample was determined by measuring the ratio of the sedimented volume of red blood cells obtained after centrifugation to the total blood volume. LCI measurements were taken while blood was flown through a glass slab capillary tube with 3 mm width and 300 μm height (World Precision Instruments,

Inc.). A programmable syringe pump (NE-501, New Era Pump Systems, Inc.) was used to flow the blood with an approximately constant speed (1mm/sec).

The slope of the LCI signal was computed and the hematocrit level was determined using a scaling factor. This scaling factor was determined using the real value of blood hematocrit. Representative LCI profiles for three different hematocrit values are shown in Figure 5.

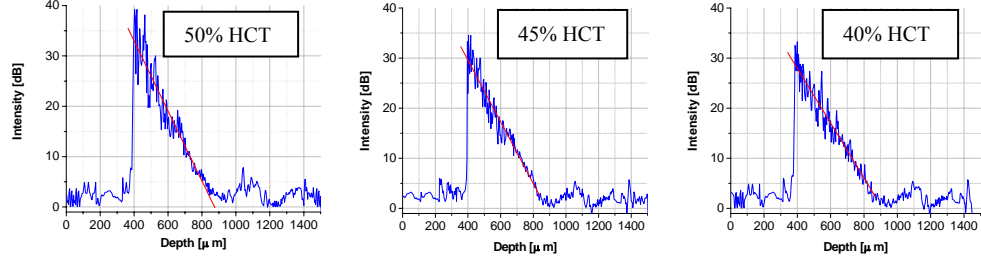


Fig. 5. LCI depth reflectivity profile for sheep blood samples with three different hematocrit ratios.

It can be noticed that the slope of the LCI signal decreases with the hematocrit decrease, which is in good agreement with the theoretical predicted behavior (see eq. (4)). A lower hematocrit means a lower scattering coefficient, and as a result a smaller LCI slope.

Statistical measurements were performed to check the stability of the slope for the same blood sample. Sets of 20 measurements on different locations of the same sample were performed and 10,000 LCI depth reflectivity profiles (A-lines) were averaged for each data set. Blood samples with hematocrit values of 35%, 40%, 45%, 50%, 55%, 60%, and 65 % were used. The results of the measurements are plotted in Fig. 6.

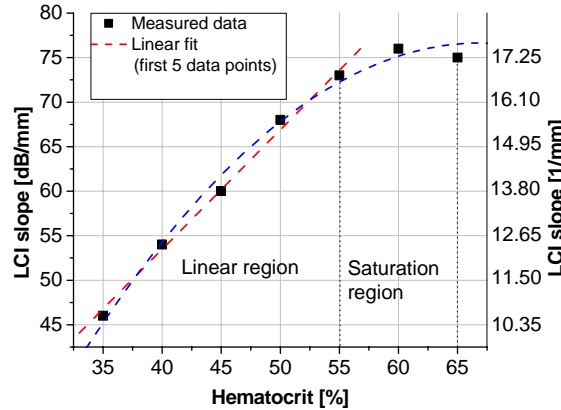


Fig. 6. Variation of the LCI slope with the hematocrit value.

The slope of the LCI reflectivity profile has almost a linear behavior for hematocrit values below 0.55, while for higher hematocrit values the slope appears to saturate and perhaps change its sign. This behavior is a consequence of the non-linear relationship between the concentration of the scatters (RBC's) and the scattering coefficient. At very high concentrations of RBC the scattering coefficient starts to saturate or even decrease. This is probable due to a percolation effect, where light effectively spends more time traversing islands of the dominant RBC phase than in plasma. A similar behavior ($H^*(1-H)$) has been described by J.M. Schmitt [3].

With regard to the value of the LCI extinction parameter, our measurements confirm the assumptions made in our theoretical model: neither the true scattering coefficient μ_s , nor the reduced value μ'_s is appropriate to be used for LCI modeling. As shown in Figure 6, a 50% hematocrit value corresponds to a slope of about 68dB/mm, which according to eq. (4) is equivalent to a total extinction coefficient of about 15.64 mm^{-1} . Considering a μ_a of about 0.8 mm^{-1} at around 800 nm [26], a $\mu_{s,LCI}$ of 14.84 mm^{-1} is obtained. This value doesn't agree with either the true scattering coefficient (about 50 to 80 mm^{-1}) or the reduced one (2 to 5 mm^{-1}) [18,26].

3.2 In vivo study

The *in vivo* study was performed on 7 healthy volunteers (4 males and 3 females) with ages between 25 and 65. The measurements were performed by accessing superficial retinal vessels and analyzing averaged one-dimensional SD-LCI axial reflectivity profiles. Eye motion stabilization was done with the TSLO instrument. Retinal LSLO images were used to localize vessels and place the LCI beam on the vessel. Multiple LCI reflectivity profiles were averaged and computed to extract the hematocrit value.

First, the capability of our system to stabilize the LCI beam on a retinal vessel was determined. With the tracking function turned “on” and “off”, both LSLO and SDOCT images were taken at 10 frames per second and the tracking accuracy was analyzed. The cross-sectional OCT images were obtained by scanning the LCI beam across the retina. A representative TSLO retinal image of a volunteer is shown in Figure 7.a). Cross-sectional OCT images of the retina for the same volunteer are shown in Figures 7.b) and 7.c). Quantitative tracking accuracy has been determined from blood vessel shadows from OCT images taken from all 7 volunteers. The maximum standard deviation in blood vessel shadow edge was less than 0.05 deg rms ($15 \mu\text{m}$) with tracking compared to approximately 0.25 deg rms without tracking but with target fixation. A similar tracking resolution was previously reported [15]. This tracking accuracy was enough to ensure that the LCI beam, with a lateral point spread function of about 25 microns, can be maintained during our measurements within the lumen of retinal vessels having at least 100 microns in diameter.

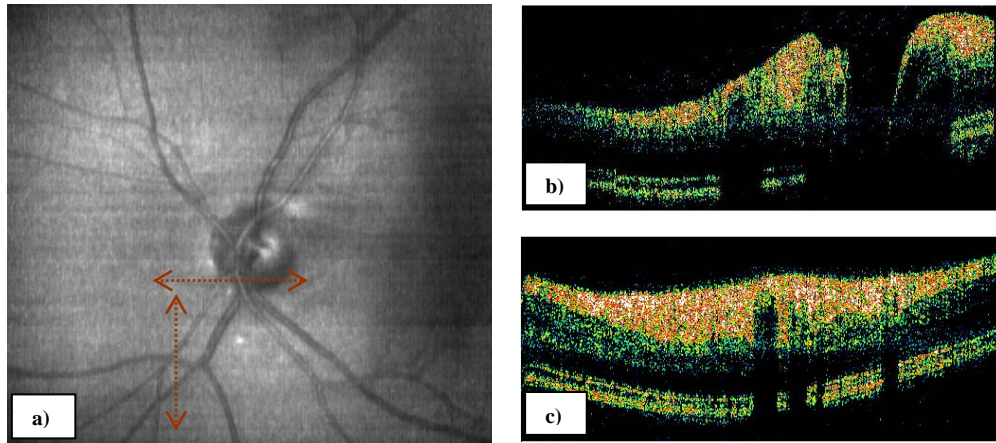


Fig. 7. a) TSLO retinal image of a volunteer. b). OCT image along the horizontal dotted line from (a). c). OCT image along the vertical dotted line from (a).

The depth of focus of the LCI/OCT beam in the eye is of the order of 1mm (twice the Rayleigh range for 25 micron beam waist at the retina). We expect that geometric focus effects over the measurable extinction range of the LCI signals ($\sim 200\mu\text{m}$) are quite small.

Further, the use of the LSLO image for focusing, whose image plane is set to be parfocal with the LCI/OCT beam, assures consistent LCI focus.

The LCI beam power was limited to less than 500 microwatts. This is orders of magnitude less than the ANSI MPE for the exposure times (a few seconds) used for non-scanning LCI measurements.

After ensuring that tracking accuracy was satisfactory for our measurements, the hematocrit study was performed. LCI reflectivity profiles were taken in major retinal vessels with diameters > 200 microns. Vessels situated in the vicinity of the nerve optic head where selected because they are close to the tracked point (typically lamina cribrosa), and allow more than 100 microns sampling depth.

Six sets of multiple LCI measurements at various time intervals were taken for each volunteer and 10,000 or more LCI depth reflectivity profiles were acquired over a second or more and averaged in each data set. The first four volunteers were males and last three were females. The slope of the reflectivity profile was extracted for each set of measurements. The variation of the slope for each individual is shown in Figure 8.a). Note that a higher slope was obtained for most of the males. The largest variation of the slope for the same individual within the six sets of measurements was 11 dB/mm (volunteer 2), which represents about 15.7% of the mean value.

The loss of LCI signal strength with depth due to the MTF of the spectrometer (~15dB) was corrected in the averaged profiles. However, some residual variation of the slope is due in part to z motion of the patient because the peak of the reflectivity profile moves within the A-line axial scan and even goes out of the measuring depth of the system. Z- tracking or automated A-scan alignment will assure that the leading edge of the lumen will always be correctly registered. These improvements will be incorporated in future work.

The hematocrit was computed from the slope of the LCI reflectivity profile using a scaling factor determined from the sheep blood measurements. However, since accompanying clinical CBCs were not included in our IRB protocol, the calibration curve and scaling factor is likely to be slightly different for human blood and as a result our present measured hematocrit values are only orientative. The only relevant correlation can be done for volunteer number 4, who has been identified as having his blood work recently performed. The hematocrit of this volunteer was pegged to the clinically measured value, approximately 42%, which is the lower normal limit for males. The estimated hematocrit value for each individual was then compared with the normal clinical range for both men and women. As shown in Fig. 8.b) our measurements indicate hematocrit values ranging within the normal limits for both males and females.

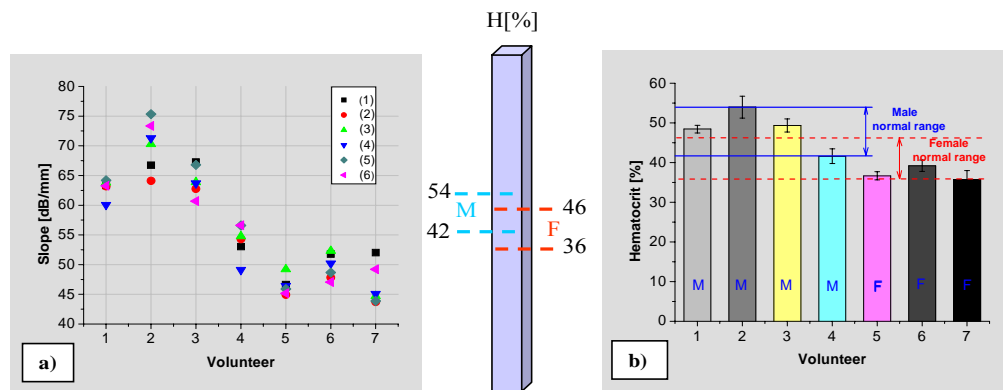


Fig. 8. a) LCI slope statistics for 7 volunteers; b) Histogram showing the correlation of the measured hematocrit with the normal clinical range.

In order to test the reproducibility of this optical method and verify our hypothesis with regard to the influence of the z motion of the eye, a new set of 8 measurements on the first volunteer was performed at a fixed z —that is, only data optimally aligned at a fixed z -range was analyzed. All 8 sets of measurements were done in exactly the same location of the retinal artery (see Figure 9.a), each comprising about 1 second of data acquired at various time intervals throughout the same day. The same calibration curve as above was used. As shown in Figure 9.b, the standard deviation of the SDLCI slope was relatively small in this case (± 0.84), which clearly is indicative of the intrinsic intra-subject precision of the technique.

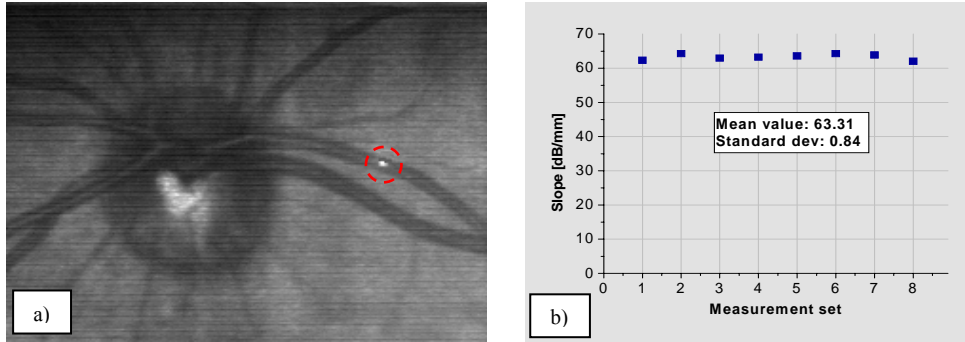


Fig.9. a) TSLO retinal image of volunteer no.1. The bright circled spot indicates the position of the LCI measurement. b) LCI slope statistics, for volunteer no.1, with head immobilization.

However, to link the measured slope to the real value of hematocrit *a priori* individual baseline data is necessary. Unfortunately, our human subjects protocol did not allow us the draw blood from volunteers to do a prompt comparison and direct calibration. This will be undertaken in future phases of this work.

4. Conclusions

This study demonstrates that precise noninvasive hematocrit measurement using SDLCI and retinal tracking is feasible. Improved calibration methods must be developed to make the measurements accurate as well. In addition, drawn blood from the investigated subjects must be used for a prompt comparison and direct calibration. This will be undertaken in future phases of this work. However, preliminary measurements on seven healthy volunteers indicate estimated hematocrit levels within the normal range for both males and females. The further development of the method and described instrumentation might allow development of a clinical tool that could be useful for daily monitoring of blood hematocrit for patients with blood disorders, and in other clinical applications. Moreover, this developing instrumentation platform can be augmented for many other physiological monitoring tasks, including blood flow, pulse profile, other *in vivo* flow cytometry applications, stimulus/response metrics of cognitive function, and others.

Acknowledgement. This work was supported by DARPA- USN-N66001-04- C-8038.